

Properties of the fluoroacrylate and methacryloxypropyl-trimethoxysilane applied to a layer of Cu₂O on bronze as either single or multi-component coatings

Luka Škrlep^{a,1}, Tadeja Kosec^a, Matjaž Finšgar^b, Andrijana Sever Škapin^a, Erika Švara Fabjan^{a,*}

^a Slovenian National Building and Civil Engineering Institute, Dimičeva ulica 12, SI-1000 Ljubljana, Slovenia

^b Faculty of Chemistry and Chemical Engineering, University of Maribor, Smetanova ulica 17, SI-2000 Maribor, Slovenia

ARTICLE INFO

Keywords:

Bronze
Cu₂O layer on bronze
Fluoropolymer coating
Protection efficiency
Surface spectroscopy

ABSTRACT

Various coatings have been developed and explored to protect bronze surfaces against the uncontrolled formation of different corrosion products when exposed to outdoor environments.

In this research, the surfaces of artificially-formed oxidized bronze patinas (OB), consisting of Cu₂O, were covered with either a single-component (fluoroacrylate, FA or methacryloxypropyl-trimethoxysilane, MS) or multi-component (a mixture of FA and MS, FA-MS) fluoropolymer coating and investigated. Variations in the concentration of each component in the coating were studied. Electrochemical tests were performed to determine the corrosion protection efficiency, followed by detailed surface analyses of the OBs, both uncoated and covered with single and multi-component coatings. A variety of investigative methods were used, including focused ion beam scanning electron microscopy (FIB-SEM), X-ray photoelectron spectroscopy (XPS), atomic force microscopy (AFM), and time-of-flight secondary ion mass spectrometry (ToF-SIMS).

The coating made from a combination of FA and MS resulted in a very high protection efficiency. Despite the increased hydrophilicity of the single MS component, however, it was shown to efficiently protect the oxidized bronze surface. The FA-MS systems showed high hydrophobicity, but no improvement was measured in the efficiency of the corrosion protection when it was compared to the coating that contained 10% MS. According to XPS and ToF-SIMS imaging, the FA component of the FA-MS coating was not present only on the uppermost surface of the coating but throughout the whole coating, which could affect its corrosion protection efficiency.

1. Introduction

The widespread use of copper and bronze over time has left us with many cultural monuments that need attention in order to preserve them for future generations. The presence of oxygen and water in the atmosphere causes the occurrence of oxidation processes on bronze surfaces, which leads to the formation of an adherent layer of copper oxides, cuprite and tenorite. In the case of more aggressive environments, further corrosion products (i.e. copper chlorides or copper sulphates) are also formed [1–3]. Bronze is one of the few alloys that can be admired even when it is completely covered with corrosion products – i.e. by the so-called patinas. The effectiveness of the protection of these patinas against further, uncontrolled, corrosion is, however, questionable, and is

dependent on many factors, including the pH value, thickness, homogeneity and adhesion of the patina [4]. Scientists have been working for years to understand the process of corrosion and find efficient ways to protect bronze artefacts, whether bare or patinated, from aggressive environments [2].

Protective organic coatings and/or inhibitors used for the purpose of conserving or restoring copper-based alloys have mainly worked by either creating a physical barrier (coatings) or forming chemical complexes (inhibitors) [5]. Waxes and varnishes (i.e. Incralac) have long been used for this purpose, but these coatings usually require constant maintenance in order to maintain a high level of effectiveness [6]. Over the past few years, scientists have proposed some new coating systems for bronze surfaces, including organosilanes [7], and protective coatings

* Corresponding author.

E-mail address: erika.svara-fabjan@zag.si (E. Švara Fabjan).

¹ Both authors equally contributed to the manuscript.

based on chitosan [8], polyurethane [9] and sodium oxalate combined with limewater [10], to improve the durability of the protection and thereby significantly extend the time required between conservation procedures. The very recent study concerns methodological overview over testing new coatings on bronze [11].

Several investigations studying the effectiveness of silane compounds in inhibiting corrosion on various copper alloys have shown that silane does not form a particularly strong bond with copper [12]. Hydrolysed propyltrimethoxysilane exhibited low protection against corrosion, while the use of a longer octyl chain on the silane enhanced the corrosion protection. The best results were achieved with mercaptopropylsilane, due to the presence of the mercapto group, which is proposed to form a strong bond with copper. This is in agreement with the investigation by Chiavari et al. [13]. One review article [14] discusses several coatings containing silane that protect against corrosion. Most solutions rely on the addition of functional groups containing N and/or S to facilitate a strong interaction with the Cu surface. One example of methyltrimethoxy silane, however, showed a stable hydrophobic effect following exposure to humidity. The nature of the bonds formed with the copper substrate was not proposed [15]. The mechanisms of protection and degradation of the mercapto functional sol-gel coating on the copper surface was investigated by Peng et al. [16], where both the mercapto group oxidation and Si—O—Si bond hydrolysis were determined.

The use of fluoropolymers for the protection of outdoor bronze was first introduced by Bierwagen et al. [17], while later the effectiveness of such coatings for the protection of patina-free and various patinated bronzes was investigated by other researchers [18–24]. The authors reported that they have several beneficial properties for use as a protective outdoor coating, including high transparency, durability in an outdoor environment, chemical resistance, good flexibility and reversibility, although such a layer exhibited a key drawback in that it had poor adhesion with the bronze surface. The weathering performance and durability of fluoropolymer films can be further improved through the addition of selected nanoparticles. Through the incorporation of chemically modified nanoclays, nanocomposite films, produced from aqueous dispersions of acrylic/ PVDF lattices, exhibit excellent weatherability and improved barrier properties [18], while the incorporation of polyhedral oligomeric silsesquioxane nanoparticles enhances the hydrophobicity and protective efficiency of fluoropolymer coatings [19]. One study tested a fluorinated elastomer on bare and patinated bronzes pretreated with various different inhibitors, namely, benzotriazole, sodium oleate, 2-mercaptobenzoxazole and tolyltriazole [20]. It was found that the best protection on bronze with a natural patina was achieved when a fluoropolymer was used in combination with an inhibitor. In order to circumvent the issue of adhesion, the authors used an acrylic basecoat primer (Paraloid® B-44) dissolved in toluene [21], or incorporated methyl methacrylate-co-methacryloxypropyltrimethoxysilane as an adhesion promotor, with promising results [22]. It seems that, with the latter solution, an efficient, reversible and non-hazardous coating, FA-MS (FA stands for fluoroacrylate, while MS is a copolymer of methyl methacrylate and methacryloxypropyltrimethoxysilane), which serves as an adhesion promotor, was developed for the protection of bare and patinated bronze exposed to outdoor conditions [23,24]. A detailed analysis of the protection efficiency (η) of FA-MS based coatings on sulphide and sulphate-patinated surfaces has already been performed by our group, and the corrosion mechanism has been suggested [25]. A lack of understanding, however, remains regarding the protection mechanism of such coatings on oxide patinated bronze i.e. oxidized bronze (OB).

The aim of this work is to investigate the corrosion protection mechanisms of FA-MS-based coatings applied to OB. For this purpose, various single- and multi-component FA-MS coatings were applied to OB, while varying the concentration of each component. Electrochemical tests were then performed to determine η , followed by detailed surface analyses of the single and multi-component coated and uncoated

OB using focused ion beam scanning electron microscopy (FIB-SEM), X-ray photoelectron spectroscopy (XPS), atomic force microscopy (AFM), and time-of-flight secondary ion mass spectrometry (ToF-SIMS).

2. Experimental

2.1. Materials

2.1.1. Sample preparation

The chemical composition of a quaternary as-cast alloy (bronze) was 88.10% Cu, 5.28% Sn, 3.84% Zn, and 2.71% Pb, all in weight percent as analyzed by arc-optical emission spectroscopy using an LMX05 SPECTRO MAXx System (SPECTRO Analytical Instruments GmbH, Kleve, Germany, 2012).

Oxidized bronze (denoted as OB) was prepared by placing a 3-mm thick, 15 mm in diameter, bronze disc on a pre-heated plate (with a temperature (T) of approx. 100 °C) for 3 min. The oxidation procedure was undertaken simultaneously on numerous samples in order to enable the formation of oxides with a similar thickness.

2.1.2. Synthesis and preparation of the coatings

The way in which the coatings were prepared has been described in detail previously [25]. Fluoropolymer (FA) was prepared by drying a commercial product (Funcosil AG, Rammers, Crawley, UK), while MS was prepared by polymerisation of methyl methacrylate and methacryloxypropyl-trimethoxysilane (9:1 M ratio). The skeletal structure of the molecules is presented in Fig. 1. All coatings use diethyl succinate and n-butyl acetate (3:2 mass ratio) as the solvent, with varying percentages of the FA and MS components, as listed in Table 1. Table 1 also displays information regarding the different characterization methods used for each sample. Only a selected number of samples underwent XPS and AFM analysis, while only one sample was chosen for FIB SEM analysis.

2.1.3. Application of the coatings on a patinated bronze surface

The coatings were applied in the same manner as described previously [25]. In all tests, a 4.4 ± 0.2 mg coating was applied to disc samples (15 mm in diameter). Before testing, the coated samples were dried for approximately 2 h under laboratory conditions and then further cured for at least 20 h at a temperature of 40 °C and relative humidity of 98%.

2.2. Methods

2.2.1. X-ray diffraction analysis (XRD)

The phase analyses of bronze and oxidized samples were determined by X-ray diffraction (XRD), using an Empyrean diffractometer (PANalytical, The Netherlands) with Cu K_{α} radiation. Powder diffraction data were collected at room temperature, at a tube tension of 45 kV and a tube current of 40 mA, using a 2θ step size of 0.013° and a measurement time of 150 s per step. Data was collected over a 2θ range of 15° to 90° . The results were analyzed using Highscore (PANalytical, Netherlands) diffraction software.

2.2.2. Surface analyses

X-ray photoelectron spectroscopy (XPS) spectra were measured using a Supra+ device (Kratos, Manchester, UK) equipped with an Al K_{α} excitation source. A charge neutraliser was switched on throughout the XPS spectra measurements. Spectra were measured at a 90° take-off angle. Gas cluster ion beam (GCIB) sputtering was performed with 10 keV Ar_{1000}^{+} . Data was collected and processed using ESCApe 1.4 software (Kratos, Manchester, UK). A binding energy scale was corrected using the C-C/C-H peak in C 1s centered at 284.8 eV. The analysis spot before and during sputtering had a diameter of 110 μ m. High-resolution spectra were acquired at a pass energy of 40 eV.

Atomic force microscopy (AFM) analyses were performed using an

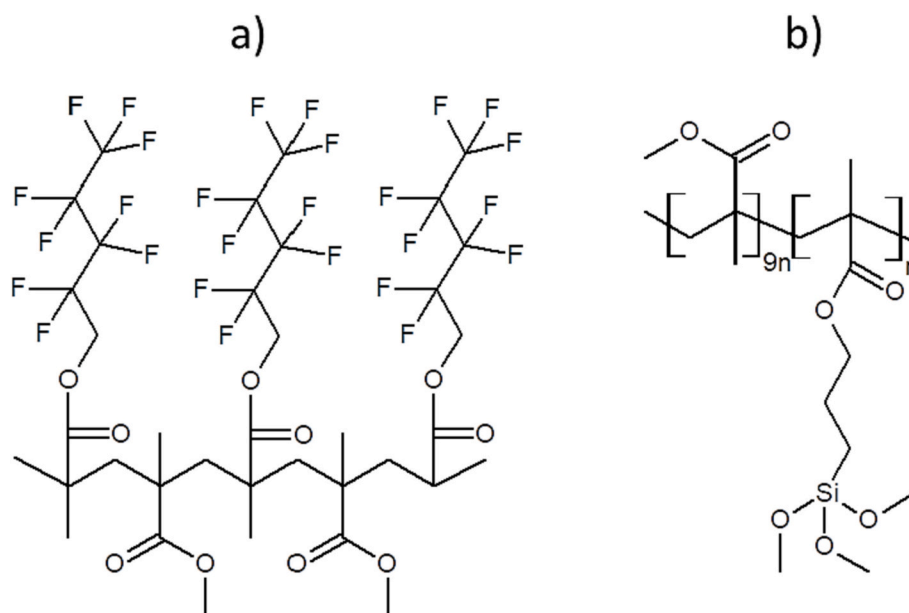


Fig. 1. Components of the fluoropolymer coating: (a) fluoroacrylate-FA and (b) methacryloxypropyl-trimethoxysilane-MS.

Table 1

Overview of the abbreviations and the characterization methods used for the various coatings applied to the oxidized bronze surfaces (percentages relate to wt%).

Abbr.	OB	Application of various coatings							
		Application of a single-component coating					Application of a double-component coating		
		Solution containing 1% MS	Solution containing 5% MS	Solution containing 10% MS	Solution containing 20% MS	Solution containing 5% FA	Solution containing 1%FA and 10%MS	Solution containing 5% FA and 10% MS	Solution containing 10% FA and 10% MS
		MS1	MS5	MS10	MS20	FA5	FA1-MS10	FA5-MS10	FA10-MS10
Characterization method used									
XRD	x								
Contact angle	x	x	x	x	x	x	x	x	x
FIB-SEM								x	
EC ^a	x	x	x	x	x	x	x	x	x
AFM		x		x		x		x	
XPS		x		x		x		x	

^a EC for electrochemical tests.

MFP 3D Origin Plus instrument (Asylum/Oxford Instruments, Santa Barbara, CA, USA) in tapping mode, with an OMCL-AC240TS-R3 silicon cantilever (Olympus Micro Cantilever, Taipei, Taiwan).

ToF-SIMS measurements were performed using an M6 device (ION-TOF, Munster, Germany) equipped with GCIB. Mass spectra were calibrated using signals at a known mass-to-charge ratio (m/z), i.e. C^- at m/z 12.00, C_2^- at m/z 24.00, C_3^- at m/z 36.00, and C_4^- at m/z 48.00. To perform 3D imaging, the surface coatings were sputtered with 5 keV Ar_{2000}^+ , followed by 10 keV Ar_{2000}^+ , over an area of 500 by 500 μm , while the analysis was performed over an area of 300 by 300 μm . The analysis beam was Bi_3^+ (30 keV), at a target current of 0.64 pA.

2.2.3. Contact angle measurements

Contact angle measurements were performed using the same method as presented in our previous work [22,25], namely the static method using an FTA 1000 DropShape Instrument B FrameSystem (First Ten Angstroms, Newark, USA). Briefly, a 2 μL droplet of deionised water was placed on the sample, then, in the next step, an image was recorded. The static contact angle was then measured by fitting the Young–Laplace equation. Three different measurements were performed in three different areas, with the average contact angle values reported as the

result.

2.2.4. FIB-SEM analysis

An FEG-SEM FEI Helios NanoLab 600i instrument with an energy dispersive X-ray spectroscopy (EDXS) detector (Aztec Oxford apparatus, SDD detector, WD 4 mm) was used to study the morphology and surface composition of the coated OB. The sample was Pt nanocoated in the range $15 \times 5 \mu m$. Cross-sections were obtained by FIB milling with Ga^+ ions. An accelerating voltage of 2 kV and a current of 12 pA were used for creating images of the surface and cross-sections.

2.2.5. Electrochemical methods

Electrochemical (EC) testing of the OB, either with or without various coatings, was conducted at 22 °C in simulated urban rain with a pH value of 5.4 and conductivity of 3.716 mS/cm. The 1000-times concentrated urban rain contained 943 mg/L NO_3^- , 686 mg/L SO_4^{2-} , and 287 mg/L Cl^- .

A Reference REF 600+ potentiostat/ galvanostat (Gamry Instruments, Warminster, US) was used for all electrochemical measurements. A three-electrode corrosion cell was used with Ag/AgCl(sat. KCl) as the reference electrode and a graphite rod as a counter electrode. All

the potentials in this work refer to the Ag/AgCl(sat. KCl) electrode.

Open circuit potential (E_{OCP}) was measured for at least 1 h, or until a stable potential was achieved. Linear polarization measurements were then conducted in the potential range ± 20 mV vs. corrosion potential (E_{corr}) at a scan rate of 0.1 mV/s. At least three replicate measurements were conducted. The average values and standard deviations were determined from scatter diagrams [26].

η was calculated using Eq. (1):

$$\eta\% = \left[1 - \left(R_p / R_p' \right) \right] \times 100 \quad (1)$$

where R_p' and R_p are the values obtained for the coated and uncoated samples, respectively, as deduced from linear polarization measurements. Polarization resistance (R_p) was defined as the slope of the tangent fitted to the curve at $j = 0$.

3. Results and discussion

3.1. Properties of the oxidized bronze

The surface of the OB sample is, according to visual observation, orange in colour (Fig. 2a). The crystal structure of the product formed on the surface was confirmed by XRD analyses using the RRUF Database (the XRD patterns for cuprite Cu_2O), as presented in Fig. 2b. The XRD pattern of cuprite (Cu_2O) shows five peaks (corresponding to the planes (110), (111), (200), (220), and (311)). All five peaks were also confirmed in the XRD pattern of the OB sample (Fig. 2b), with some of them overlapping with the XRD pattern for pure bronze. The arrows in Fig. 2b indicate the non-overlapping peaks and confirm the presence of cuprite (Cu_2O) on the surface of the OB sample.

3.2. Properties of the coated oxidized bronze

3.2.1. FIB-SEM

The surface of the OB was covered with a layer of various single- or double-component coatings (Table 1). A FIB-SEM micrograph of the cross-section of one coating (FA5-MS10) applied to the surface of the OB is presented in Fig. 3. The cross-section micrograph of the Cu_2O layer shows it is 350 nm to 900 nm thick with an uneven and rough surface. Naturally developed cuprite patinas, however, can be up to a few μm thick. Results of this study answer some mechanistic aspects of corrosion protection efficiency of the coatings, but do not necessarily represent the same protection efficiency as if used on natural cuprite patinas. The FA5-

MS10 coating (i.e. the upper layer) covered the patinated surface smoothly and evenly. As already observed in our previous work [22], an air bubble was trapped in the coating (see the interface coating- Cu_2O layer in Fig. 3).

3.2.2. AFM

AFM images of the various coatings, with the corresponding mean surface roughness (S_a), are presented in Fig. 4. The FA5 coating, MS1, MS10, and double-component coating, FA5-MS10, are presented at the same scale. Where MS was applied, the 10 wt% MS coating formed a continuous and smooth layer ($S_a = 2$ nm), while in MS1 a higher roughness was observed ($S_a = 27$ nm). The FA5 coating also smoothly covered the surface of the oxidized bronze ($S_a = 5$ nm), while some discontinuity was observed when the two-component coating (FA5-MS10) was applied ($S_a = 7$ nm).

3.2.3. Contact angle

The contact angles for OB before and after application of the coatings are presented in Table 2. The contact angle of the uncoated OB was 99° . Following application of the MS coating the contact angle was lower, indicating the hydrophilic properties of the MS coating. The lowest value corresponds to the most concentrated sample, MS20, where the contact angle is 75° . It can be seen that an increase in the concentration of the MS component leads to an increase in hydrophilicity. In contrast, the application of a single-component fluoropolymer coating (FA5) resulted in increased hydrophobicity, with an increased contact angle of 114° in comparison to the contact angle of 99° in the uncoated OB.

The contact angles for the double-component coatings were very similar to that of the single fluoropolymer coating (FA), regardless of the variation in concentrations (values between 115° and 116°), suggesting that the upper layer of the double-component coating consisted of the FA component.

3.2.4. Evaluation of η for the various coatings

E_{OCP} was measured alongside the linear polarization measurements in order to evaluate the electrochemical properties of the coated oxidized bronze. Fig. 5 shows the scatter diagram with error bars (standard deviations) of the logarithmic values of R_p for OB and the various protection systems. The values of E_{OCP} , average R_p values, and calculated η values are listed in Table 3. One replicate of the linear polarization curve measurements is presented in Supplementary material.

The E_{OCP} potential of OB did not change much over time, whether

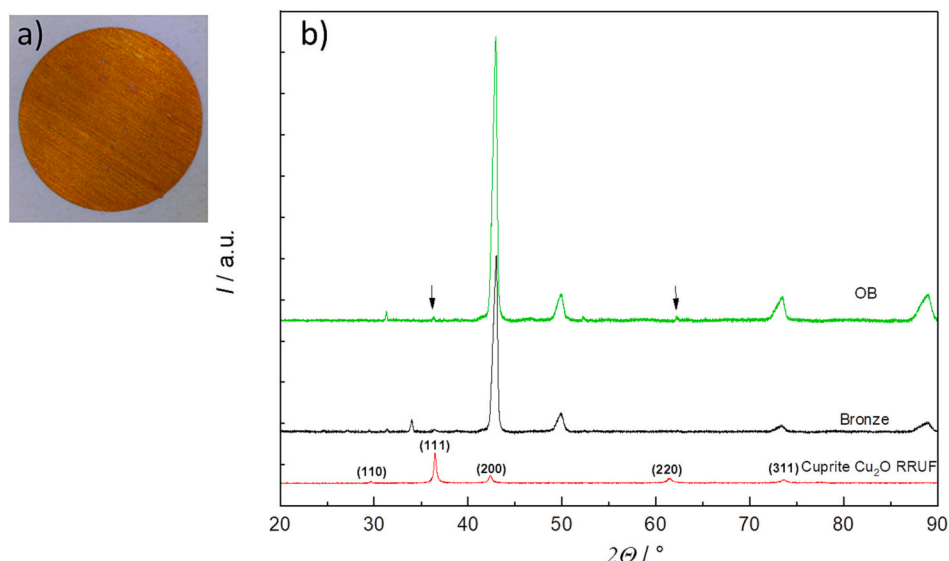


Fig. 2. a) Photograph of the OB sample, b) XRD patterns of the bronze sample, OB, and cuprite (Cu_2O RRUF).

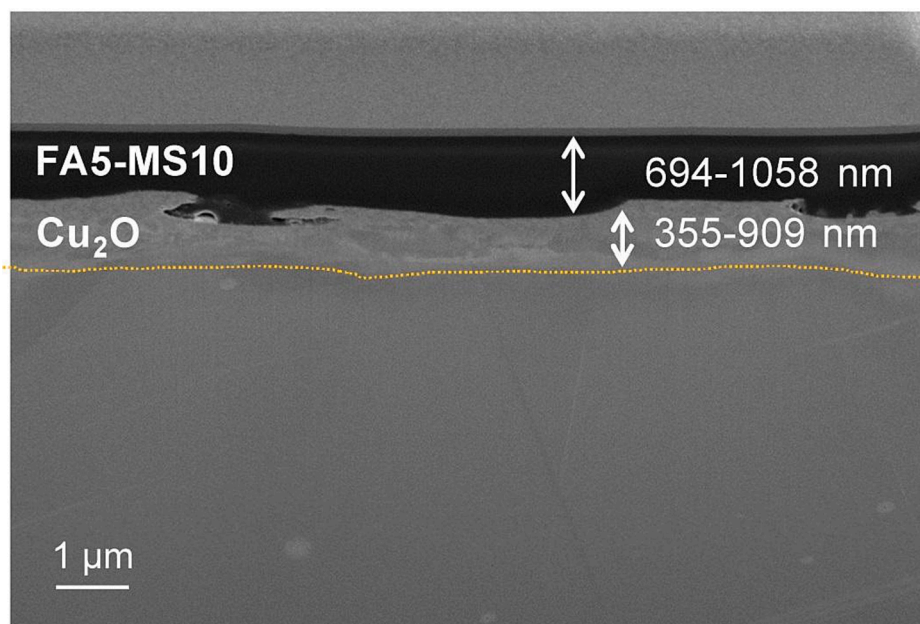


Fig. 3. FIB-SEM micrograph of the FA5-MS10 coating on oxidized bronze.

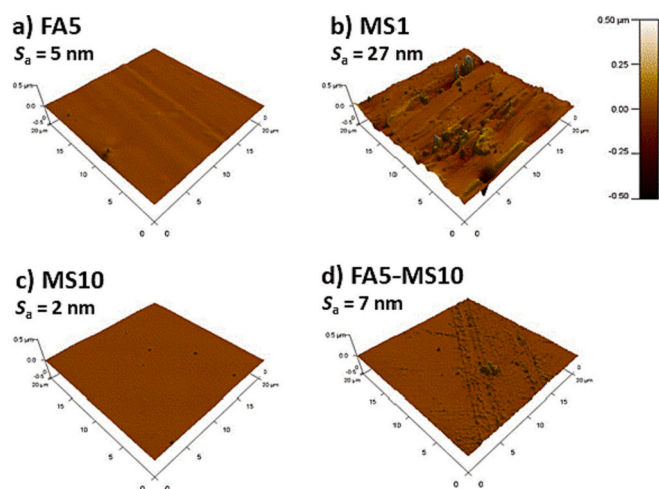


Fig. 4. AFM micrographs of a) FA5, b) MS1, c) MS10 and d) FA5-MS10 applied to OB.

Table 2

Contact angle values in the various samples following application of the various coatings.

Sample	Sample/coating	Contact angle/°
Unprotected patina	OB	99 ± 7
Single-component coating	MS1	86 ± 5
	MS5	78 ± 1
	MS10	77 ± 1
	MS20	75 ± 1
	FA5	114 ± 2
Multiple-component coating	FA1-MS10	116 ± 1
	FA5-MS10	116 ± 0
	FA10-MS10	115 ± 1

with or without a coating applied. After 1 h of immersion the E_{OCP} was around 0 mV, with variations of ± 20 mV for the OB coated with MS1 or MS5 and -20 mV for the OB coated with MS20 (Fig. 5a). The R_p of the uncoated OB was $24 \text{ k}\Omega \text{ cm}^2$. When MS was applied as a coating at

varying concentrations (1, 5, 10, and 20 wt%) the R_p increased, resulting in values of η of 99.5% and 99.6% for MS10 and MS20, respectively. OB coated with MS1 had the lowest R_p value (Fig. 5b, Table 3). Increasing the concentration of MS in the solution from 1 to 20 wt% increased the R_p value from $55 \text{ k}\Omega \text{ cm}^2$ to $12,300 \text{ k}\Omega \text{ cm}^2$. The application of FA5 only slightly increased the R_p value compared to the uncoated OB, reaching a value of η of 36.6%. The use of combinations of coatings, MS10-FAx (where $x = 1, 5,$ and 10), resulted in very high R_p values. An increase in the concentration of FA, on the other hand, does not have an impact on the value of η . Linear polarization measurements for OB and the various coatings are presented in Fig. S1 in the Supplementary material.

3.2.5. XPS analyses

XPS analysis was performed on the MS1 and MS10 coatings in order to investigate the effect of the wt% concentration of the MS component in the solvent in the single-component coating, and on FA5 and FA5-MS10 in order to define the surface properties of FA and a mixture of FA and MS in the double-component coating system.

3.2.5.1. MS1-coated OB. Fig. 5 shows high-resolution spectra measured before and after sputtering with 10 keV Ar_{1000}^+ . Before sputtering (represented by the lowest spectra in Fig. 6), the surface was not rich in Cu-containing species, since the surface was coated with MS1. Sputtering with GCIB effectively removed the coating, and a more intense signal was obtained for Cu-containing species (Fig. 6-a and b). As the satellites in the Cu 2p spectra were missing (they should be located at the dashed lines in Fig. 6a), it can be concluded that no Cu(II)-species were present on the surface. The XPS-excited Auger $\text{Cu}_{3L_{4,5}}\text{M}_{4,5}$ spectrum after 15 s of sputtering corresponds to Cu_2O , with peak 1 being the most intense. Further sputtering (up to 60 s) led to the increase in peak 2, as more metallic Cu was obtained (Fig. 6b). The lowest C 1s spectrum, representing the sample's uppermost position, contains spectral features corresponding to C—C/C—H, C=O, and COO species. Sputtering with GCIB increased the signal for COO (Fig. 6c). Moreover, before sputtering, the O 1s spectrum showed two different O chemical environments (represented by the dashed lines 1 and 2 in Fig. 6d). The intense feature at a more negative E_B (marked by dashed line 2) can correspond to the O species in the MS1 coating (such as O in C=O/COO groups). The spectral feature at dashed line 1 becomes more intense during sputtering and most likely corresponds to the O atoms attached to Si in the MS1

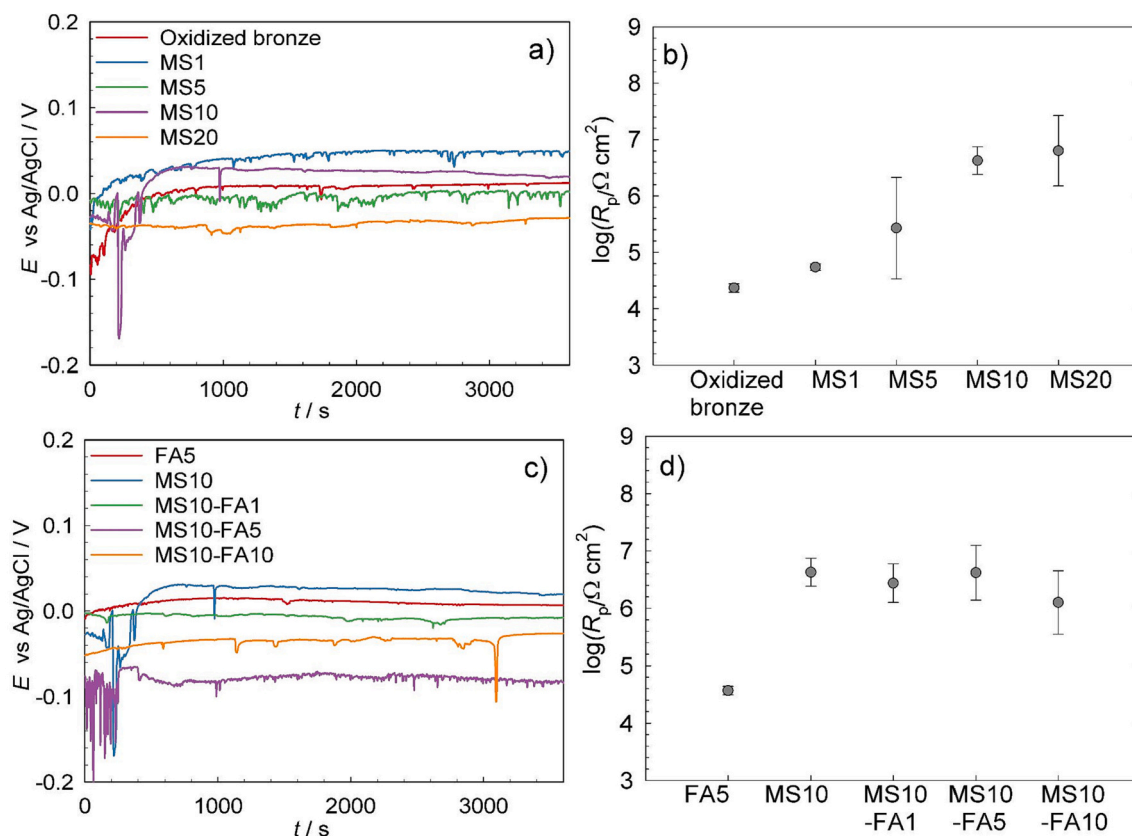


Fig. 5. E_{OCP} measurements (a, c), and average R_p values along with standard deviations (b, d) for the OB both with and without the various types of protective coating (MS1, MS5, MS10, MS20, FA5, MS10, MS10-FA1, MS10-FA5, and MS10-FA10).

Table 3

Electrochemical parameters; E_{corr} (read from Fig. 5), average R_p values, and η , calculated using Eq. (1).

Sample	Sample/ coating	$E_{corr}/$ mV	Average $R_p/k\Omega$ cm^2	$\eta/\%$
Unprotected patina	Oxidized bronze	14.7	23	–
Single component coating	MS1	50.9	55	57 ± 6
	MS5	11.7	270	80 ± 25
	MS10	15.7	4260	99.4 ± 0.3
	MS20	–22.6	6350	99.4 ± 0.6
Double component coating	FA5	6.64	37	36 ± 11
	FA1-MS10	–7.74	2750	99.0 ± 0.7
	FA5-MS10	–84.4	4180	99.3 ± 0.7
	FA10-MS10	–26.1	1270	97 ± 3

which were involved in bonding MS to the surface. A peak in the Si 2p spectrum at 101.7 eV (Fig. 6e) before sputtering confirms that the MS1 coating was successfully applied to the substrate.

3.2.5.2. MS10-coated OB. XPS analysis of the M10-coated sample is shown in Fig. 7. The substrate has the same structure as the MS1-coated sample i.e. Cu_2O is present on the sample's surface below the coating, without the presence of Cu(II) species (Fig. 7, a and b). On the other hand, the C 1s spectra (Fig. 7c) show that the spectral feature for COO-containing species become less intense when the sputtering time is increased. The O 1s spectra (Fig. 7d) show the same environment as described for the MS1 coating. As expected, the MS10 coating is thicker than MS1, where sputtering was needed for more than 1020 s was

needed so that the peak in the Si 2p spectra becomes less intense (Fig. 7e).

3.2.5.3. FA5-coated OB. Application of the FA5 coating did not change the surface properties of the substrate. Beneath the coating, the sample's surface was composed of Cu_2O (spectrum after 75 s sputtering), without the presence of Cu(II) species (Fig. 8a and b). Sputtering for more than 75 s increased the spectral feature 2 compared to spectral feature 1 in the XPS-excited Auger $Cu_{3L_{4,5}}M_{4,5}$ spectra, indicating that a more intense signal was obtained from metallic Cu (Fig. 8b). In addition to the C 1s spectra for the MS1 and MS10 coatings, the C 1s spectra for the FA5 coating contained additional peaks at a more positive E_B compared to the peak for COO-containing species. These additional peaks represent F-containing species for CF_2 and CF_3 (Fig. 8c). An intense signal was also found in the F 1s spectra before sputtering (Fig. 8d). By sputtering, the peak in the F 1s spectra became less intense. O 1s spectra for the FA5-coated OB (Fig. 8e) show less resolved peaks at dashed lines 1 and 2 compared to the O 1s spectra for the OB coated with either MS1 (Fig. 6d) or MS10 (Fig. 7d). The spectral features do, however, appear at a similar position as in the case of the samples coated with MS1 and MS10.

3.2.5.4. FA5-MS10-coated OB. As with the other three samples discussed above, the sample's surface (i.e. the bare substrate) was covered with Cu_2O following application of the FA5-MS10 coating (results not shown). The chemical environment of C atoms for the FA5-MS10 coating was similar to that of the FA5 coating (Fig. 9a vs. Fig. 8c). The signal representing F-containing species in Fig. 9b was present up until 2100 s of sputtering. Two different O environments were identified for the FA5-MS10 coated sample i.e. the uppermost position (the lowest spectra) with O-containing species in the MS coating (marked at the dashed line 2), and O-containing species located in the deeper subsurface region (marked at dashed line 1), corresponding to O atoms involved in

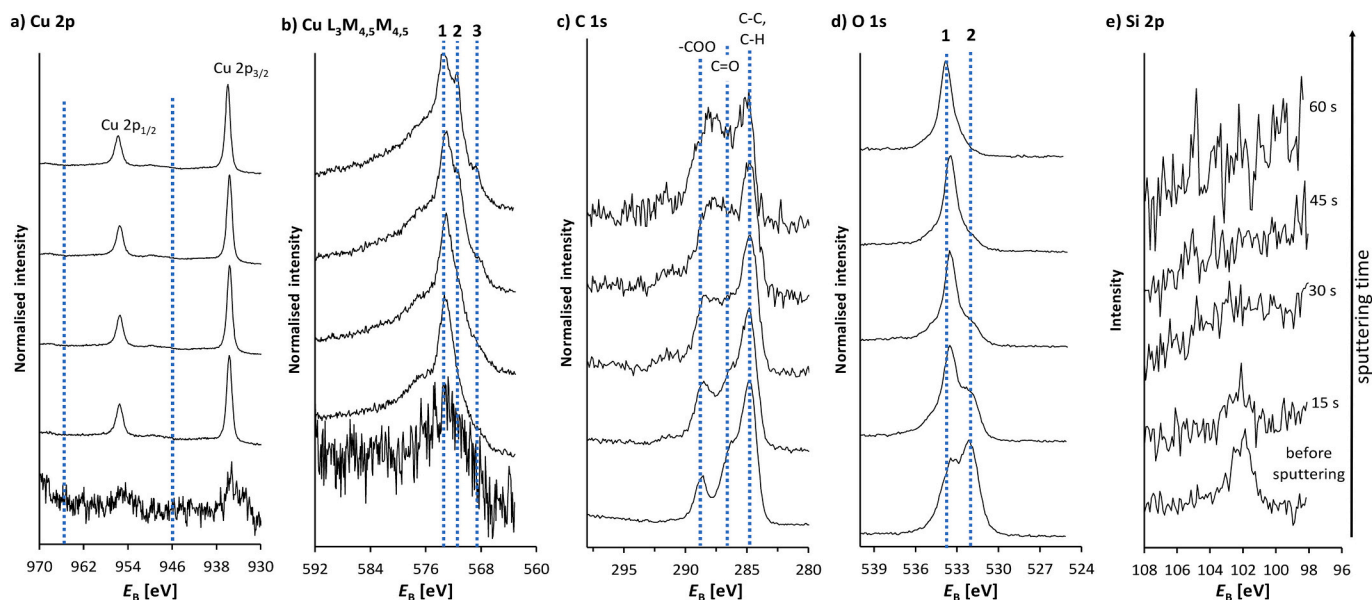


Fig. 6. HR XPS a) C 1s, b) XPS-excited Auger $\text{Cu}_3\text{L}_{4.5}\text{M}_{4.5}$, c) C 1s, d) O 1s, and e) Si 2p spectra for the MS1 coating. The sputtering time is shown in e).

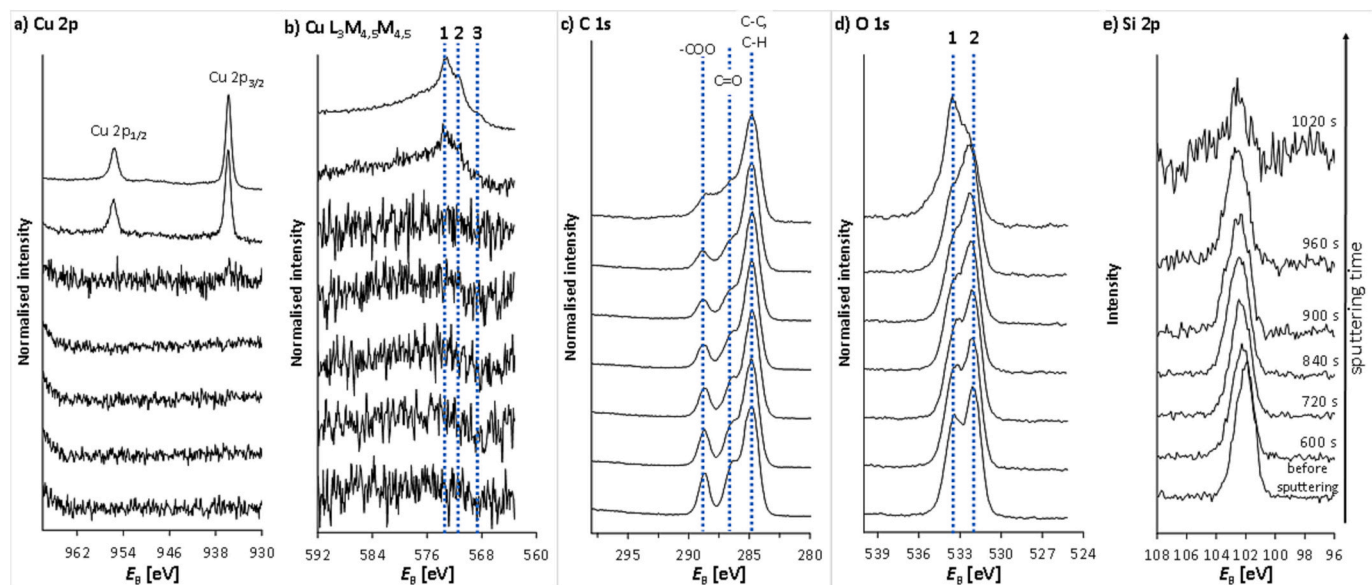


Fig. 7. HR XPS a) C 1s, b) XPS-excited Auger $\text{Cu}_3\text{L}_{4.5}\text{M}_{4.5}$, c) C 1s, d) O 1s, and e) Si 2p spectra for the MS10 coating. The sputtering time is shown in e).

bonding MS to the surface (Fig. 9c). The signal for Si-containing species was not present in the uppermost position, but appeared after 420 s and was then present up to 1680 s of sputtering. After 2100 s of sputtering, the peak in Si 2p spectra disappeared, due to the removal of the MS layer. On the other hand, the peak in the F 1s spectrum was still present after 2100 s, as the FA layer is underneath the MS layer.

3.2.6. 3D ToF-SIMS imaging

The surface distribution of the coating species and substrate was determined by 3D ToF-SIMS imaging (Fig. 10). The surface species are represented by the signals in negative polarity measured for SiO_3^- at m/z 75.96, F^- at m/z 19.00, CF_3^- at m/z 68.99, and Cu^- at m/z 62.93. SiO_3^- represents the distribution of the MS coatings, while the signals for F^- (inside FA5) and CF_3^- (terminal groups in FA5) represent the FA5 coating. The substrate is represented by the signal for Cu^- . Sputtering started at 5 keV Ar_{2000}^+ (upper 3D images in Fig. 8), followed by 10 keV Ar_{2000}^+ (lower 3D images in Fig. 10). Sputtering with 5 keV Ar_{2000}^+ shows

a uniform distribution of the MS1 and MS10 coatings (green areas in the 3D images) on the substrate (red areas, representing Cu^- , Fig. 10). The transition from green areas (MS1 and MS10 coatings) to red areas (substrate) is not sharp in the 3D images, as the substrate was ground, leaving the surface with scratches that were filled with the coating. When the substrate was coated with FA5, the uppermost species represented terminal CF_3 groups (black areas), followed by F-containing species (blue areas). The FA5/substrate interface was similar to that of the MS/substrate interfaces i.e. there were scratches filled with the coating. As also described above for the sample coated with FA5-MS10 examined using XPS, the SIMS image (Fig. 10) shows that the uppermost position of the surface is rich in F-containing species (signal for F^- , blue areas), followed by Si-containing species below (SiO_3^- , green areas). Moreover, F-containing species were located in deeper subsurface regions (inside the substrate scratches).

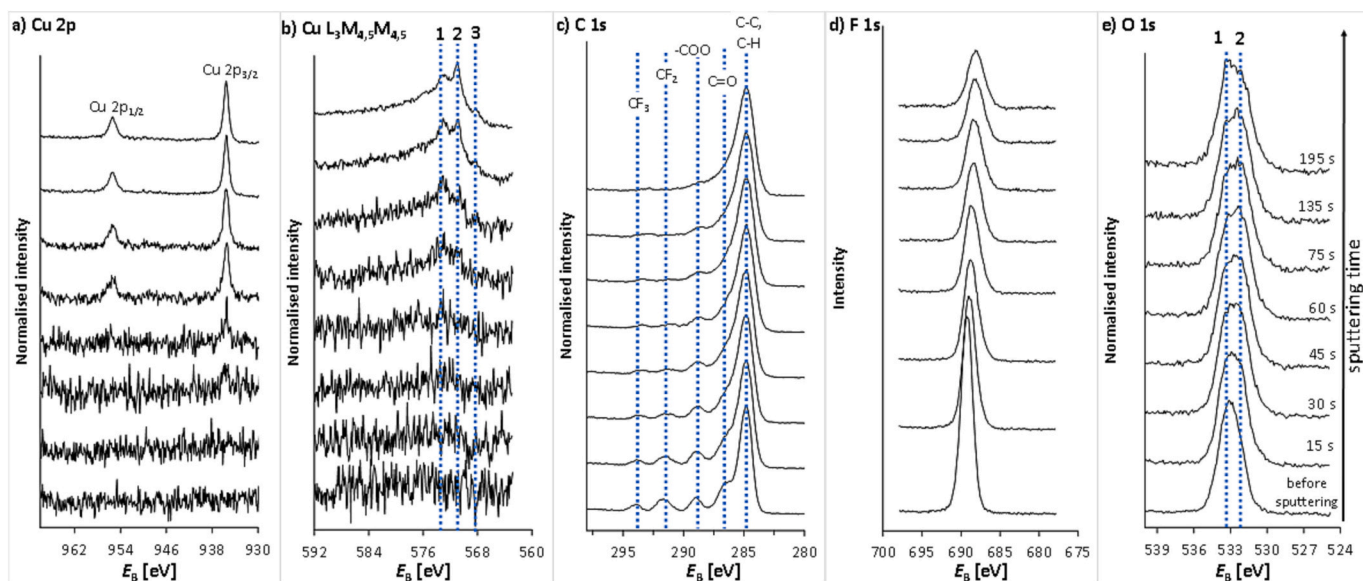


Fig. 8. HR XPS a) C 1s, b) XPS-excited Auger $\text{Cu}_{3L_{4,5}M_{4,5}}$, c) C 1s, d) F 1s, and e) O 1s spectra for the FA5 coating. The sputtering time is given in e).

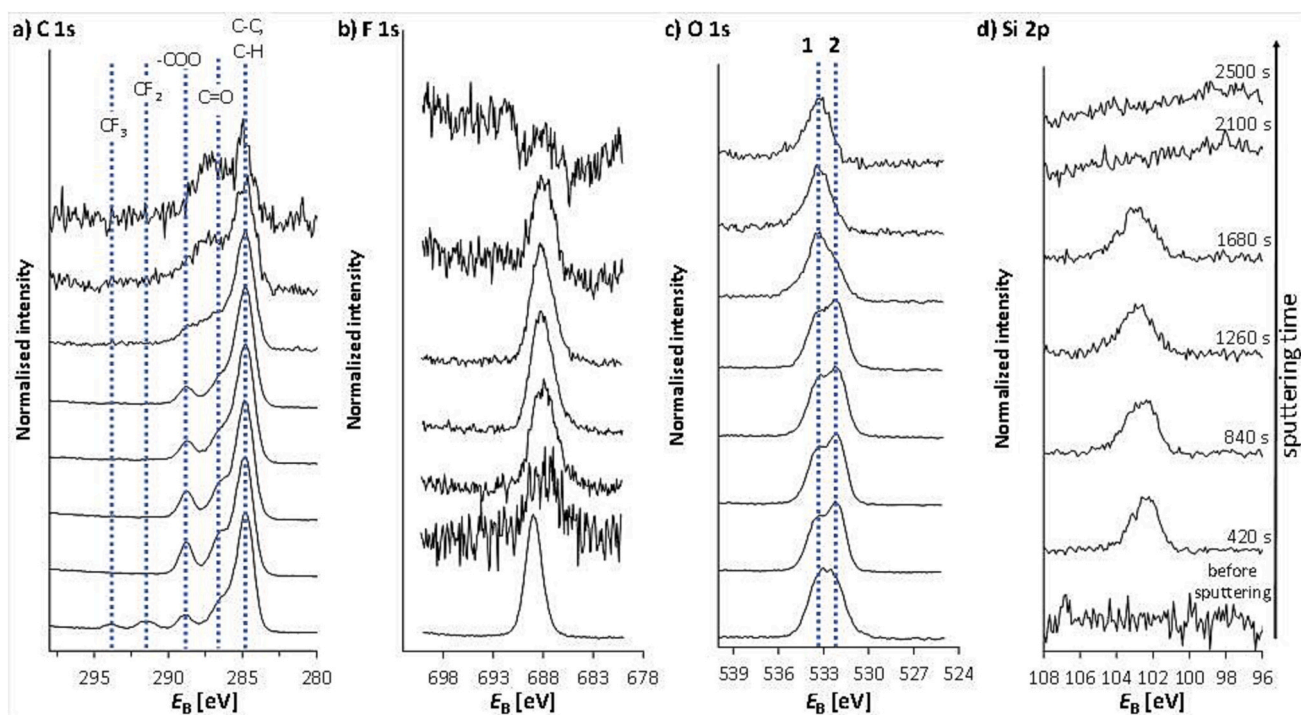


Fig. 9. HR XPS a) C 1s, b) F 1s, c) O 1s, and d) Si 2p spectra for the FA5-MS10 coating. The sputtering time is given in d).

4. Conclusion

The aim of the present work was to determine the properties of the fluoroacrylate-FA or methacryloxypropyl-trimethoxysilane-MS or multi-component (a mixture of FA and MS, FA-MS) protection system on bronze and to find its mechanisms of protection against corrosion by determining the structure and orientation of the molecules in the coating, relating to the protection efficiency of the coating. Various coatings, including FA and MS and combinations thereof, were applied to OB and investigated using a variety of experimental methods. It was determined that the FA coating alone does not offer sufficient protection against corrosion, despite high hydrophobicity. The MS component shows very efficient concentration-dependent corrosion protection of up

to about 10%, despite having low contact angles. By combining FA and MS systems, effective corrosion protection efficiency was retained when compared to MS alone, while providing desirable high contact angles.

The GCIB sputtering associated with XPS analysis showed that the surface of the coated and non-coated OB substrate does not contain Cu (II) species. Moreover, successful application of the Si- and F-containing coatings was confirmed by GCIB-XPS analyses. Furthermore, the ToF-SIMS technique enabled the identification of elemental- and molecular-specific signals, which showed the spatial distribution of F^- , SiO_3^- , and Cu-related species (represented by the Cu^- signal), and CF_3^- (representing terminal groups of the FA coating). It was shown that CF_3 groups in the FA coating were positioned towards the outer interface of the coating, offering the desirable property of high hydrophobicity.

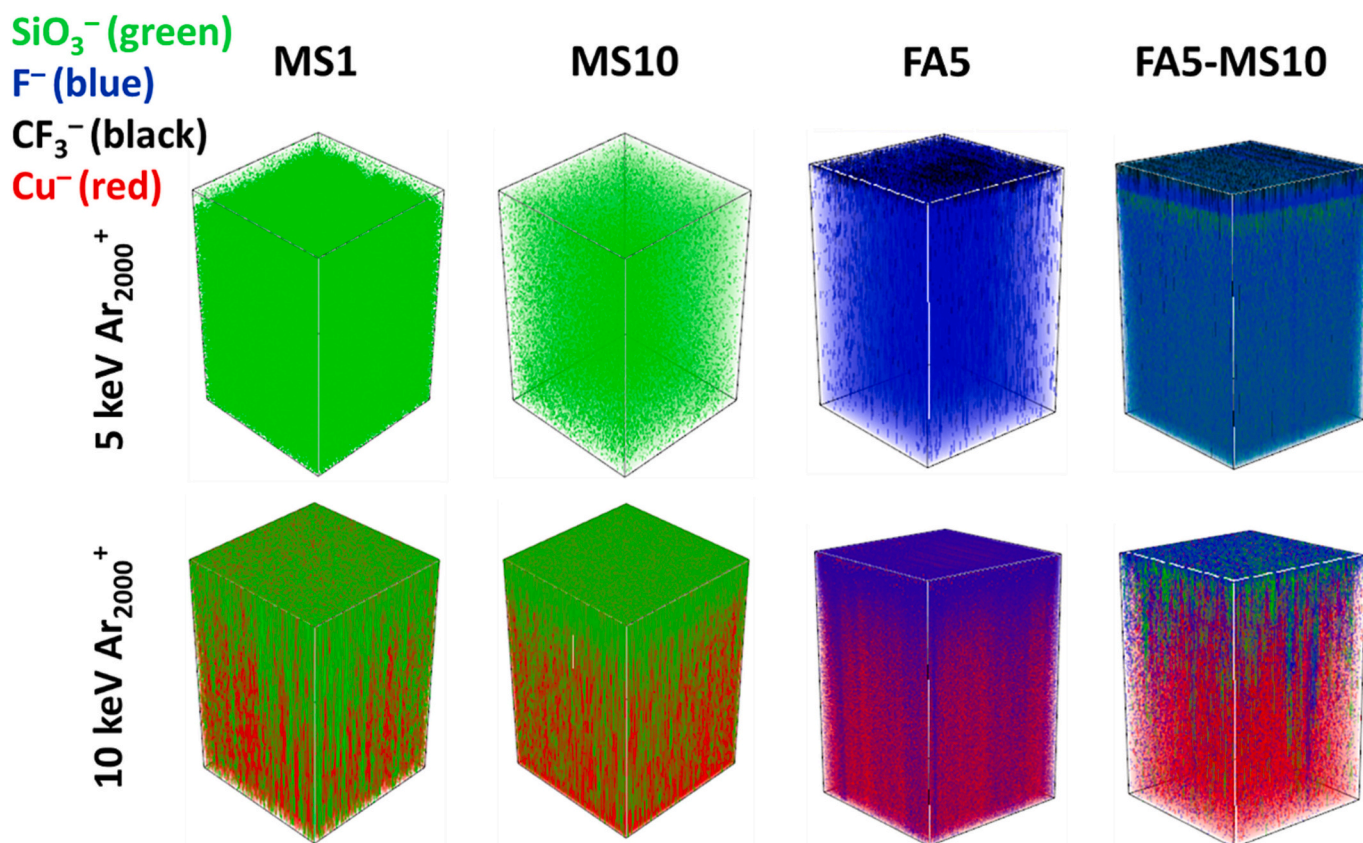


Fig. 10. ToF-SIMS 3D-imaging performed by sputtering with 5 keV Ar_{2000}^+ followed by 10 keV Ar_{2000}^+ . The sputtering crater was made on an area of 500 by 500 μm , while the analysis spot (x- and y-direction) was 300 by 300 μm . The distance in the z-direction is not proportional to the x- and y-directions.

Supplementary data to this article can be found online at <https://doi.org/10.1016/j.porgcoat.2023.107440>.

CRediT authorship contribution statement

Luka Škrlep: Conceptualization, Formal analysis, Writing – review & editing. **Tadeja Kosec:** Investigation, Writing – review & editing, Formal analysis, Supervision, Funding acquisition. **Matjaž Finšgar:** Formal analysis, Writing – original draft, Writing – review & editing. **Andrijana Sever Škapin:** Writing – original draft, Writing – review & editing. **Erika Švara Fabjan:** Conceptualization, Validation, Writing – original draft, Writing – review & editing.

Declaration of competing interest

The authors declare that they have no known competing financial interests or personal relationships that could have appeared to influence the work reported in this paper.

Data availability

Data will be made available on request.

Acknowledgments

The financial support received from the Slovenian Research Agency (SRA) for programmes P2-0273 and P2-0118 and project NK-0001 is hereby gratefully acknowledged. The project is co-financed by the Republic of Slovenia, the Ministry of Education, Science and Sport, and the European Union through the European Regional Development Fund.

References

- [1] D.A. Scott, *Copper and Bronze in Art: Corrosion, Colorants, Conservation*, The Getty Conservation Institute, Los Angeles, 2003.
- [2] A. Krättschmer, I. Odneval Wallinder, C. Leygraf, The evolution of outdoor copper patina, *Corros. Sci.* 44 (2002) 425–450, [https://doi.org/10.1016/S0010-938X\(01\)00081-6](https://doi.org/10.1016/S0010-938X(01)00081-6).
- [3] F. Ospitali, C. Chiavari, C. Martini, E. Bernardi, F. Passarini, L. Robbiola, The characterization of sn-based corrosion products in ancient bronzes: a Raman approach, *J. Raman Spectrosc.* 43 (2012) 1596–1603, <https://doi.org/10.1002/jrs.4037>.
- [4] C. Chiavari, K. Rahmouni, H. Takenouti, S. Joiret, P. Vermaut, L. Robbiola, Composition and electrochemical properties of natural patinas of outdoor bronze monuments, *Electrochim. Acta* 52 (2007) 7760–7769, <https://doi.org/10.1016/j.electacta.2006.12.053>.
- [5] P. Dillmann, G. Beranger, P. Piccardo, H. Matthiessen, *Corrosion of Metallic Heritage Artefacts: Investigation, Conservation and Prediction of Long Term Behaviour*, Elsevier Science, 2014.
- [6] E. Sandell, *New Materials for the Coating of Outdoor Bronze*, Columbia University, 2018. Thesis, M.S.
- [7] G. Masi, C. Josse, J. Esvan, C. Chiavari, E. Bernardi, C. Martini, M.C. Bignozzi, C. Monticelli, F. Zanotto, A. Balbo, E. Švara Fabjan, T. Kosec, L. Robbiola, Evaluation of the protectiveness of an organosilane coating on patinated Cu-Si-Mn bronze for contemporary art, *Prog. Org. Coat.* 127 (2019) 286–299, <https://doi.org/10.1016/j.porgcoat.2018.11.027>.
- [8] C. Giuliani, M. Pascucci, C. Riccucci, E. Messina, M. Salzano de Luna, M. Lavorgna, G.M. Ingo, G. Di Carlo, Chitosan-based coatings for corrosion protection of copper-based alloys: a promising more sustainable approach for cultural heritage applications, *Prog. Org. Coat.* 122 (2018) 138–146, <https://doi.org/10.1016/j.porgcoat.2018.05.002>.
- [9] M. Mihelčić, M. Gaberšček, G. Di Carlo, C. Giuliani, M. Salzano de Luna, M. Lavorgna, A.K. Surca, Influence of silsesquioxane addition on polyurethane-based protective coatings for bronze surfaces, *Appl. Surf. Sci.* 467–468 (2019) 912–925, <https://doi.org/10.1016/j.apsusc.2018.10.217>.
- [10] G. Monari, M. Galeotti, M. Matteini, B. Salvadori, R. Stifanese, P. Traverso, S. Vettori, P. Letardi, Protective treatments for copper alloy artworks: preliminary studies of sodium oxalate and limewater effectiveness against bronze disease, *Environ. Sci. Pollut. Res. Int.* (2022), <https://doi.org/10.1007/s11356-022-24107-0>.
- [11] P. Letardi, Testing new coatings for outdoor bronze monuments: a methodological overview, *Coatings* 11 (2021) 131, <https://doi.org/10.3390/coatings1102013>.

- [12] F. Zucchi, V. Grassi, A. Frignani, G. Trabaneli, Inhibition of copper corrosion by silane coatings, *Corros. Sci.* 46 (2004) 2853–2865, <https://doi.org/10.1016/j.corsci.2004.03.019>.
- [13] C. Chiavari, A. Balbo, E. Bernardi, C. Martini, M.C. Bignozzi, M. Abbottoni, C. Monticelli, Protective silane treatment for patinated bronze exposed to simulated natural environments, *Mater. Chem. Phys.* 141 (2013) 502–511, <https://doi.org/10.1016/j.matchemphys.2013.05.050>.
- [14] J. Balaji, P.B. Raja, M.G. Sethuraman, T.H. Oh, Recent studies on sol–gel based corrosion protection of Cu—A review, *J. Sol-Gel Sci. Technol.* 103 (2022) 12–38, <https://doi.org/10.1007/s10971-022-05818-9>.
- [15] A.V. Rao, S.S. Latthe, S.A. Mahadik, C. Kappenstein, Mechanically stable and corrosion resistant superhydrophobic sol–gel coatings on copper substrate, *Appl. Surf. Sci.* 257 (2011) 5772–5776, <https://doi.org/10.1016/j.apsusc.2011.01.099>.
- [16] S. Peng, J. Han, W. Zhao, Z. Zeng, J. Chen, X. Wu, The protection and degradation behaviors of mercapto functional sol-gel coating on copper surface, *J. Electrochem. Soc.* 162 (2015) C128–C134, <https://doi.org/10.1149/2.0091504jes>.
- [17] G. Bierwagen, T.J. Shedlosky, K. Stanek, Developing and testing a new generation of protective coatings for outdoor bronze sculpture, *Prog. Org. Coat.* 48 (2003) 289–296, <https://doi.org/10.1016/j.porgcoat.2003.07.004>.
- [18] N.A. Swartz, C.A. Price, T. Lasseter Clare, Minimizing corrosion of outdoor metalworks using dispersed chemically stabilized nanoclays in polyvinylidene fluoride latex coatings, *ACS Omega* 1 (1) (2016) 138–147, <https://doi.org/10.1021/acsomega.6b00091>.
- [19] M. Mihelčić, M. Gaberšček, C. Giuliani, G. Di Carlo, A.K. Surca, M. Salzano de Luna, M. Lavorgna, Effect of silsesquioxane addition on the protective performance of fluoropolymer coatings for bronze surfaces, *Materials & Design* 178 (2019) 107860, <https://doi.org/10.1016/j.matdes.2019.107860>.
- [20] B. Salvadori, A. Cagnini, M. Galeotti, S. Porcinai, S. Goidanich, A. Vicenzo, C. Celi, P. Frediani, L. Rosi, M. Frediani, G. Giuntoli, L. Brambilla, R. Beltrami, S. Trasatti, Traditional and innovative protective coatings for outdoor bronze: application and performance comparison, *J. Appl. Polym. Sci.* 135 (2018) 46011, <https://doi.org/10.1002/APP.46011>.
- [21] N.A. Swartz, A.K. Wood, T. Lasseter Clare, Characterizing and improving performance properties of thin solid films produced by weatherable water-borne colloidal suspensions on bronze substrates, *Prog. Org. Coat.* 75 (2012) 215–223, <https://doi.org/10.1016/j.porgcoat.2012.04.017>.
- [22] T. Kosec, L. Škrlep, E. Švara Fabjan, A. Sever Škapin, G. Masi, E. Bernardi, C. Chiavari, C. Josse, J. Esvan, L. Robbiola, Development of multi-component fluoropolymer based coating on simulated outdoor patina on quaternary bronze, *Prog. Org. Coat.* 131 (2019) 27–35, <https://doi.org/10.1016/j.porgcoat.2019.01.040>.
- [23] T. Kosec, Ž. Novak, E. Švara Fabjan, L. Škrlep, A. Sever Škapin, Corrosion protection of brown and green patinated bronze, *Prog. Org. Coat.* 161 (2021) 106510, <https://doi.org/10.1016/j.porgcoat.2021.106510>.
- [24] G. Masi, E. Bernardi, C. Martini, I. Vassura, L. Škrlep, E. Švara Fabjan, N. Gartner, T. Kosec, C. Josse, J. Esvan, M.C. Bignozzi, L. Robbiola, C. Chiavari, An innovative multi-component fluoropolymer-based coating on outdoor patinated bronze for cultural heritage: durability and reversibility, *J. Cult. Herit.* 45 (2020) 122–134, <https://doi.org/10.1016/j.culher.2020.04.015>.
- [25] T. Kosec, Ž. Novak, E. Švara Fabjan, L. Škrlep, M. Finšgar, Exploring the protection mechanism of a combined fluoropolymer coating on sulphide patinated bronze, *Prog. Org. Coat.* 172 (2022) 107071, <https://doi.org/10.1016/j.porgcoat.2022.107071>.
- [26] W.S. Tait, *An Introduction to Electrochemical Corrosion Testing for Practicing Engineers and Scientists*, PairODocs Publications, Racine, USA, 1994.